Optical Response of Graphene Under Strain

Master's Thesis, 31.12.2021

Author:

Amr Mousa

Supervisors:

Risto Ojajärvi
Tero Heikkilä

UNIVERSITY OF JYVÄSKYLÄ
DEPARTMENT OF PHYSICS

Abstract

Strain has been known to modify the electric and optical properties of graphene. This phenomenon has attracted interest to modifying graphene properties using specific forms of strains (known as strain-engineering), and measuring strain in graphene. In this thesis, I present a calculation of the optical properties of strained graphene, where the effects of strain can be seen in the optical conductivity and thus the reflectivity of graphene.

To do this, I use the tight-binding model to obtain the Dirac Hamiltonian of the charge carriers in graphene. Then I deduce the effects of in-plane strain as a pseudo-magnetic field potential and use this result to add strain as a perturbation to the Hamiltonian of pristine graphene.

Using the perturbed Hamiltonian, I calculate the optical conductivity of graphene for a specific strain field with a y-component that is periodic in x. I obtain the optical conductivity numerically for different amplitudes of the strain, and use them to find the reflectivity.

The results indicate that the effects of strain on reflectivity can be measured experimentally, and that such measurements can reveal information about the amplitude and period of the strain.

Mousa, Amr
Master's thesis
Department of Physics, University of Jyväskylä, 2021, 50 pages.

keywords: optical response of graphene, strained graphene, optical conductivity of graphene, graphene reflectivity

Contents

1 Introduction

In 2004, Graphene was the first atomically-thin material discovered [1], and it has since been subject of active research due to its interesting electric and mechanical qualities. Graphene consists of a single layer of carbon atoms arranged in a hexagonal lattice. In spite of its extremely small thickness, graphene is an extremely strong material with respect to its resilience to strain. Experiments have confirmed the extremely high intrinsic breaking strength graphene is theorized to have [2].

In addition to its strength, graphene has attracted interest due to its electrical properties. Electron transport in graphene has been shown to obey Dirac's equation; the relativistic equation for fermions. Experiments confirmed [3] that charge carriers in graphene behave like Dirac fermions with zero rest mass (or effective mass), and a constant speed $c = 10^6$ m/s analogous to the speed of light at which massless particles travel in vacuum.

Optical properties of graphene are also interesting; experiments measuring the optical response of graphene have confirmed the theoretical prediction (which I outline below) that the transparency of graphene depends directly on the fine-structure constant α [4].

While this is true for pristine graphene, studying the optical response of graphene under strain is the main goal of this study. Interest in strained graphene have given rise to the field of strain-engineering in graphene which is the study of modifying the electric and optical properties of graphene using strain [5]. This has had applications such as strain-sensors where graphene is used to measure strain on surfaces [6], as well as the possibility of graphene becoming superconducting under strain [7].

In this thesis, I study the effect of in-plane strain on the conductivity and reflectivity of graphene, and present numerical calculations for the case of periodic strain. In Chapter 2, I introduce Bloch's theorem along with the graphene lattice. I then briefly explain the tight-binding model and use it to show the reciprocal lattice and the Dirac Hamiltonian for graphene.

In Chapter 3, I introduce strain and show that the displacement of atoms in the lattice has an effect that can be treated like a pseudo-magnetic field. Then I show the gauge freedom of the strain field where some strain profiles correspond to the

same electron dispersion and therefore the same electronic properties.

In Chapter 4, I discuss a specific strain profile, namely strain in the y-direction that is periodic in the x-direction. I arrive at the Hamiltonian for Dirac fermions in graphene under the given strain. Then, in Chapter 5, I deduce the expressions for the optical conductivity and reflectivity.

Chapter 6 outlines the numerical methods used to calculate the optical conductivity and reflectivity using the Hamiltonian obtained in chapter 4 and the equations arrived at in chapter 5, and present the results from the numerics.

2 Graphene basics

In order to study the optical properties of graphene as well as the effects of strain on them, we must first study the lattice of pristine graphene. In this chapter, I introduce the graphene hexagonal lattice and the tight-binding model which is used to find the energy eigenstates, the dispersion relation and finally express the Hamiltonian of the graphene charge carriers as massless Dirac fermions.

2.1 Bloch's theorem

In solids, atoms organize in crystals as they form chemical bonds with neighbouring atoms; since the atoms' nuclei are much more massive than electrons, they can be mostly treated as stationary. In the lattice they provide a periodic potential for the electrons. An important result dealing with periodic potentials is Bloch's theorem, which states that solutions to the Schrödinger equation in periodic potentials must be of the form [8]

$$\psi_k(r) = u_k(r)e^{ik\cdot r}, \tag{1}$$

where

$$u_k(r+T) = u_k(r), \tag{2}$$

where k is the wave vector and T is any lattice vector. A lattice vector is a vector that expresses the translational symmetry of the lattice such that for any point r on the lattice, the atomic arrangement looks the same at a point r' given by

$$r' = r + T. \tag{3}$$

Any lattice vector can be expressed in terms of the basis lattice vectors a_1, and a_2 in the form

$$T = u_1 a_1 + u_2 a_2, \tag{4}$$

where u_1 and u_2 are integers, and a choice of basis vectors is shown in figure 1 below. Then for the wave function we have the condition

$$\psi_k(r+T) = u_k(r+T)e^{ik\cdot r}e^{ik\cdot T} = \psi_k(r)e^{ik\cdot T}, \tag{5}$$

and functions with this property are known as Bloch Functions. Bloch's theorem is used below for both pristine graphene and periodically strained graphene.

2.2 The graphene lattice

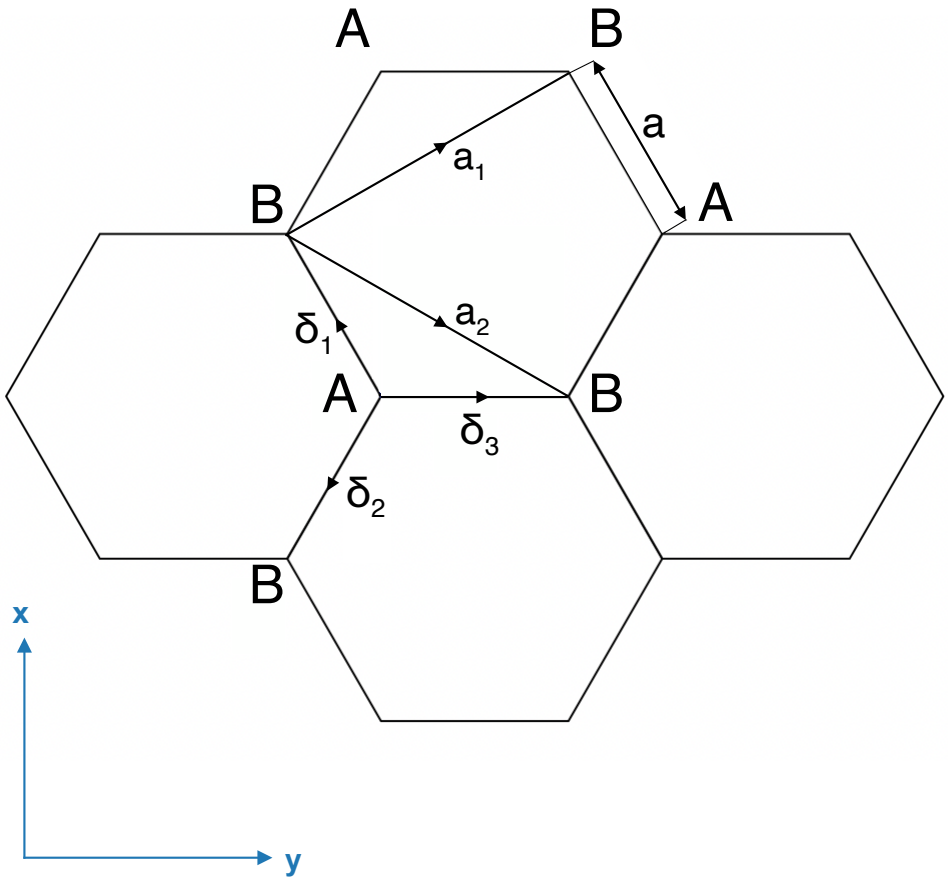

Figure 1. Hexagonal lattice of graphene

The graphene lattice shown in Fig. 1 has a honeycomb shape with the nearest-neighbor distance $a \approx 1.42$Å [9]. The elementary cell consists of two atoms A and B, connected by the nearest-neighbor vectors

$$\delta_{1,2} = \mp\frac{\sqrt{3}a}{2}\hat{u}_x - \frac{a}{2}\hat{u}_y, \qquad \delta_3 = a\hat{u}_y, \tag{6}$$

as shown in the figure. The lattice vectors connecting elementary cells are a_1, and a_2, where

$$a_1 = \frac{a}{2}(\sqrt{3}, 3) \qquad a_2 = \frac{a}{2}(-\sqrt{3}, 3). \tag{7}$$

Using the lattice vectors and nearest-neighbor vectors, we can infer the interactions between lattice sites and construct a model for describing the dynamics of the charge carriers in graphene; so next, this model is described along with the resulting Hamiltonian.

2.2.1 Tight-binding model

An approximation often used to treat electrons in graphene is the tight-binding approximation where the wave functions of electrons bound to free atoms are considered and modified as atoms are brought closer together into the lattice [8]. Given the electronic wave functions ϕ, the tight-binding Hamiltonian is

$$H(r) = \sum_{m,n} \int dV \phi^*(r + r_m) H \phi(r + r_n) \tag{8}$$

for all atom sites m and n. It should be noted that the volume integral above is two-dimensional in graphene. Including only the nearest-neighbor atoms is a good approximation. In this case we have the Hamiltonian for one A atom

$$H(r) = \sum_{j}^{3} \int dV = \phi^*(r) H \phi(r + \delta_j) \tag{9}$$

The term $\int dV \phi^*(r) H \phi(r + \delta_j) = -\gamma_0$ is the same for all j as long as δ_j's have the same magnitude, due to the symmetry of the lattice. The Hamiltonian can now be written in terms of γ_0, known as the hopping parameter, and electronic creation and destruction operators in the form

$$\hat{H}_g(R) = -\gamma_0 \sum_R \sum_{j=1}^{3} \hat{\psi}^\dagger(R) \hat{\psi}(R + \delta_j) + h.c. \tag{10}$$

where $\hat{u}_x, \hat{u}_y$ are the basis vectors as shown in figure 1, and the R sum runs over all lattice sites. Then we can write the Fourier transform of the wave functions

$$\psi(R) = \frac{1}{\sqrt{N}} \sum_k e^{-ik\cdot R} c_{k,A}, \tag{11}$$

and

$$\psi(R+\delta_j) = \frac{1}{\sqrt{N}} \sum_k e^{-ik\cdot R} e^{-ik\cdot\delta_j} c_{k,B}, \tag{12}$$

where $c_{k,A/B}$, and $c^\dagger_{k,A/B}$ are the destruction/creation operators for electrons in A/B sites, and N is the number of lattice sites.

Using equations (11) and (12), we can re-write the Hamiltonian as

$$\hat{H}_g = -\gamma_0 \frac{1}{N} \sum_R \sum_{k,k'} c^\dagger_{k,A} e^{iR\cdot(k-k')} (\sum_{j=1}^{3} e^{-ik\cdot\delta_j}) c_{k',B} + h.c. \tag{13}$$

Since

$$\sum_R e^{iR\cdot(k'-k)} = N\delta_{kk'},$$

we have

$$\hat{H}_g = \sum_k c_{k,A}[-\gamma_0(\sum_{j=1}^{3} e^{-ik\cdot\delta_j})] c^\dagger_{k,B} + h.c. \tag{14}$$

Defining γ_k as

$$\begin{aligned}
\gamma_k &= -\gamma_0(\sum_{j=1}^{3} e^{-ik\cdot\delta_j}) \\
&= -\gamma_0 e^{-ik_y a}[1 + e^{i(k_x \frac{\sqrt{3}}{2}a + k_y \frac{3}{2}a)} + e^{i(-k_x \frac{\sqrt{3}}{2}a + k_y \frac{3}{2}a)}] \\
&= -\gamma_0 e^{-ik_y a}[1 + 2e^{ik_y \frac{3}{2}a} \cos\left(k_x \frac{\sqrt{3}}{2}a\right)],
\end{aligned} \tag{15}$$

we can re-write equation (14) as

$$\hat{H}_g = \sum_k \begin{pmatrix} c^\dagger_{k,A} & c^\dagger_{k,B} \end{pmatrix} \begin{pmatrix} 0 & \gamma_k \\ \gamma^*_k & 0 \end{pmatrix} \begin{pmatrix} c_{k,A} \\ c_{k,B} \end{pmatrix}. \tag{16}$$

Defining the matrix $H_g = \begin{pmatrix} 0 & \gamma_k \\ \gamma^*_k & 0 \end{pmatrix}$, we can write the characteristic equation

$$(H_g - \epsilon_k I) = 0. \tag{17}$$

This has the solutions

$$\epsilon_k = \pm|\gamma_k|, \tag{18}$$

which gives us the equation for the eigenenergies

$$\epsilon_k = \mp\gamma_0\sqrt{1 + 4\cos^2\left(k_x\frac{\sqrt{3}}{2}a\right) + 4\cos\left(k_x\frac{\sqrt{3}}{2}a\right)\cos\left(k_y\frac{3}{2}a\right)}. \tag{19}$$

Given the eigenenergies, the Hamiltonian can be expressed in the form of an expansion around specific eigenenergies and eigenstates. In the next section I express the Hamiltonian as an expansion up to first order around the zero energy states known as momentum valleys.

2.3 Dirac hamiltonian in graphene

2.3.1 Reciprocal lattice

The reciprocal lattice is the momentum-space equivalent of the given position-space lattice, with the condition that for the reciprocal lattice basis vectors b_1 and b_2 we have [8]

$$a_i \cdot b_j = 2\pi\delta_{ij}. \tag{20}$$

From equations (19) and (15) the values of k for which $\epsilon_k = 0$ are given by solving the equation

$$\gamma_k = 0 \tag{21}$$

which gives us

$$e^{ik_y\frac{3}{2}a}\cos k_x\frac{\sqrt{3}}{2}a = -\frac{1}{2}. \tag{22}$$

Since the right hand side is real, then $e^{ik_y\frac{3}{2}a} = \pm 1$, which implies

$$k_y = n\frac{2}{3a}\pi, \tag{23}$$

where $n = 0, \pm1, \pm2, \pm3, \ldots$. Then we have $\cos k_x\frac{\sqrt{3}}{2}a = \pm\frac{1}{2}$, which implies

$$k_x = m\frac{2}{3\sqrt{3}a}\pi. \tag{24}$$

where $m = \pm1, \pm2, \pm4, \pm5, \ldots$, i.e. m is a non-zero integer not divisible by 3, and is even when n is even and odd when n is odd, in order to maintain the sign in equation (21). This gives the reciprocal lattice with lattice points $K = \frac{2\pi}{3a}(\frac{1}{\sqrt{3}},1)$, and $K' = \frac{2\pi}{3a}(-\frac{1}{\sqrt{3}},1)$ (equivalent to points A and B in position space) as shown in figure

2.

It is easily verified that reciprocal lattice vectors

$$b_1 = \frac{2\pi}{3a}(\frac{3}{\sqrt{3}},1), \qquad b_2 = \frac{2\pi}{3a}(-\frac{3}{\sqrt{3}},1), \tag{25}$$

and the lattice vectors given in equation (6) satisfy the condition (20). The same is true for points $K + v_1b_1 + v_2b_2$ and $K' + v_1b_1 + v_2b_2$ for any integers v_1 and v_2.

Next, we expand the Hamiltonian to linear order in momentum around K. Since

$$\gamma_k = -\gamma_0 e^{-ik_y a}[1 + 2e^{ik_y \frac{3}{2}a} \cos{(k_x \frac{\sqrt{3}}{2}a)}],$$

we have

$$\frac{\partial}{\partial k_x}\gamma_k(K) = -\gamma_0 \alpha \frac{3}{2}a,$$

while

$$\frac{\partial}{\partial k_y}\gamma_k(K) = i\gamma_0 \alpha \frac{3}{2}a,$$

where $\alpha = e^{-i\frac{2\pi}{3}}$.

Similarly we get

$$\frac{\partial}{\partial k_x}\gamma_k^*(K) = -\gamma_0 \alpha^* \frac{3}{2}a,$$

and

$$\frac{\partial}{\partial k_y}\gamma_k^*(K) = -i\gamma_0 \alpha^* \frac{3}{2}a.$$

Then we have

$$\hat{H}_g^k \approx -\gamma_0 \frac{3}{2}a \begin{pmatrix} 0 & \alpha[(k_x - K_x) - i(k_y - K_y)] \\ \alpha^*[(k_x - K_x) + i(k_y - K_y)] & 0 \end{pmatrix},$$

since we can remove the phase α with a unitary transformation, we can reduce the Hamiltonian to the form

$$\hat{H}_g^k \approx -\gamma_0 \frac{3}{2}a \begin{pmatrix} 0 & (k_x - K_x) - i(k_y - K_y) \\ (k_x - K_x) + i(k_y - K_y) & 0 \end{pmatrix},$$

Equation (2.3.1) can be written as

$$\hat{H}_g^k \approx v_F \sigma \cdot (\boldsymbol{k} - \boldsymbol{K}),$$

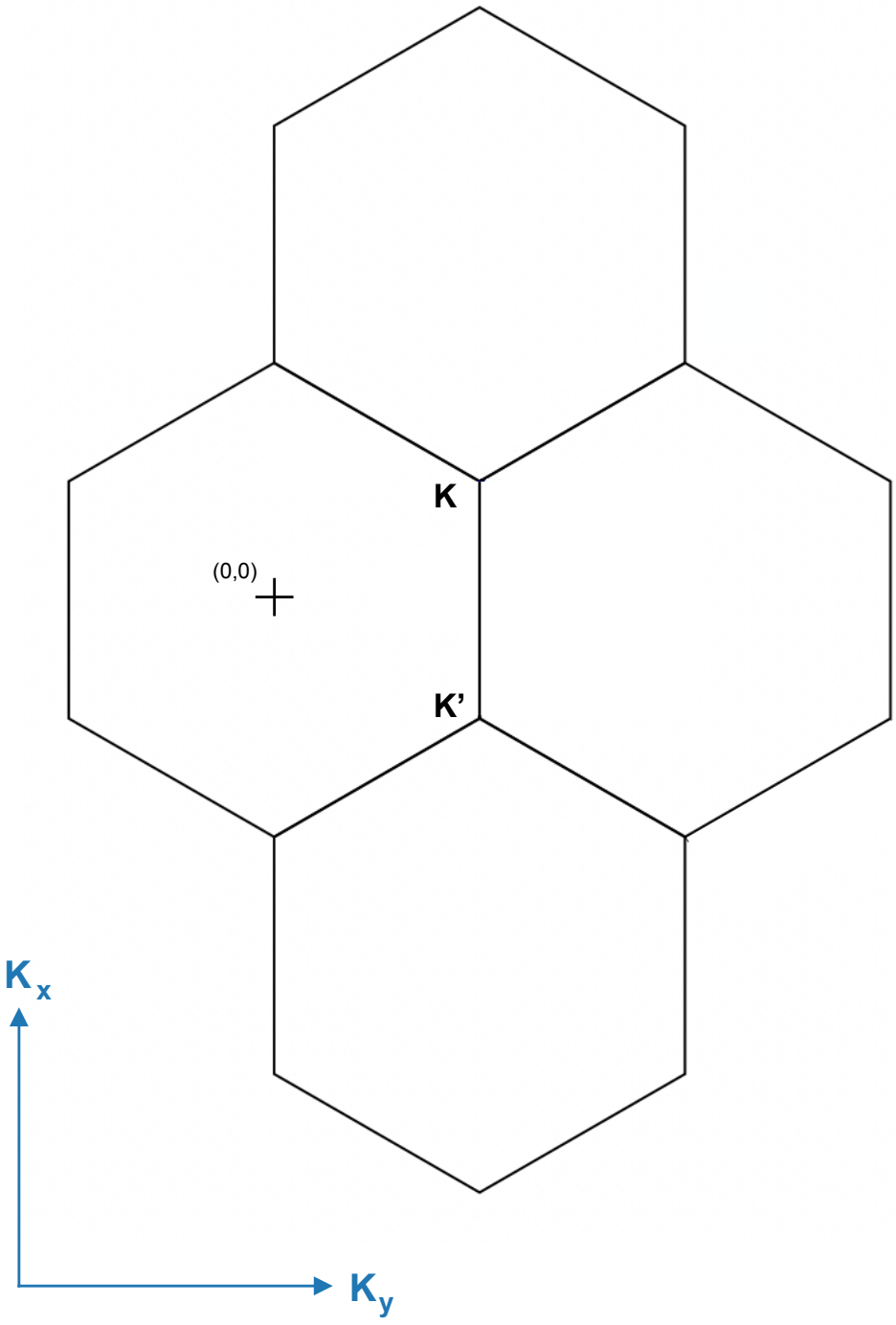

Figure 2. Reciprocal lattice

or using the shorthand notation $q = k - K$

$$\hat{H}_g^k \approx v_F \sigma \cdot q, \tag{26}$$

where $\sigma = \begin{pmatrix} \sigma_x & \sigma_y \end{pmatrix}$ are the Pauli matrices, $\boldsymbol{k} = \begin{pmatrix} k_x & k_y \end{pmatrix}$, and $v_F = -\gamma_0 \frac{3}{2} a$. In a similar way, expanding around K' gives

$$\hat{H}_g^{k'} \approx \gamma_0 \frac{3}{2} a \begin{pmatrix} 0 & (k_x - K'_x) + i(k_y - K'_y) \\ (k_x - K'_x) - i(k_y - K'_y) & 0 \end{pmatrix}$$

$$\hat{H}_g^{k'} \approx -v_F \sigma^* \cdot q, \tag{27}$$

where $q = k - K'$ here. The corresponding eigenstates for electrons and holes are [9]

$$\psi_{e,h}^{(K)}(q) = \frac{1}{\sqrt{2}} \begin{pmatrix} e^{-i\frac{\theta}{2}} \\ \pm e^{i\frac{\theta}{2}}, \end{pmatrix} \tag{28}$$

where θ is the angle of the momentum in polar coordinates (i.e. $\vec{q} = (q\cos\theta, q\sin\theta)$), while for the K' valley, we have [9]

$$\psi_{e,h}^{(K')}(q) = \frac{1}{\sqrt{2}} \begin{pmatrix} e^{i\frac{\theta}{2}} \\ \pm e^{-i\frac{\theta}{2}} \end{pmatrix}. \tag{29}$$

It is easy to confirm that these are eigenstates of the Hamiltonian in equations (26), and (27), with eigenenergies

$$\epsilon = \pm v_f q. \tag{30}$$

Given the description of the electron/hole states and the Hamiltonian, it is now possible to introduce a perturbation to the Hamiltonian corresponding to the strain profile. In the next section, I study the effect of strain on the Hamiltonian.

3 Strain in graphene

Strain in graphene is often measured with the help of Raman spectroscopy, i.e. detecting inelastic photon scattering from graphene [6]. In this section, I describe a different approach where strain can be recognised through its effects on the optical properties of monolayer graphene. This is done by first demonstrating that the effect of strain on graphene can be represented as an electromagnetic pseudo-vector, and then finding the forms of strain which would have no effect on the optical properties of graphene. In this thesis, I concentrate on in-plane strain.

3.1 Strain as a pseudo-magnetic field

Applying strain to a graphene sheet changes the inter-atomic spacing and thus modifies the hopping parameters such that they are no longer the same for all neighbouring atoms. The displacement field

$$u(x,y) = (u_x(x,y), u_y(x,y)) \tag{31}$$

denotes the x and y displacements of a lattice site from its original position before strain. Then the hopping parameters up to the first order in the displacement vectors become [10]

$$\gamma_n = \gamma_0(1 - \beta\frac{\delta_n^i \delta_n^j}{a^2}u_{ij}), \tag{32}$$

where δ_n^i is the ith component of the nearest neighbour vectors δ^i defined above, $\beta = \frac{\partial \log \gamma_0}{\partial \log a}$ is the Grüneisen parameter, and $u_{ij} = \frac{1}{2}(\partial_i u_j + \partial_j u_i)$ is the strain tensor. The Einstein summation notation is used whenever an index is repeated as a lower and upper index. Equation (15) becomes

$$\gamma_k = -\gamma_0(1 - \beta\frac{\delta_n^i \delta_n^j}{a^2}u_{ij})(\sum_{j=1}^{3} e^{-ik\cdot\delta_j}) = \gamma_k^{'} + \tilde{\gamma}_k, \tag{33}$$

where $\gamma_k^{'}$ is the value for non-strained graphene while $\tilde{\gamma}_k$ is the extra term. For the point $K = \frac{2\pi}{3a}(\frac{1}{\sqrt{3}},1)$ we get

$$\tilde{\gamma}_K = \sum_{n=1}^{3} \gamma_0 \frac{\beta}{a^2}\delta_n^i \delta_n^j u_{ij} e^{-iK\cdot\delta_n}. \tag{34}$$

To evaluate $\tilde{\gamma_k}$, we note that

$$\begin{aligned} K \cdot \delta_1 &= \frac{-2\pi}{3} \\ K \cdot \delta_2 &= 0 \\ K \cdot \delta_3 &= \frac{2\pi}{3}. \end{aligned} \tag{35}$$

Then we get

$$\tilde{\gamma_K} = \gamma_0 \frac{\beta}{a^2}[u_{xx}(\frac{3}{4}a^2)(e^{i\frac{2\pi}{3}}+1)]+[u_{yy}\frac{1}{4}a^2(e^{i\frac{2\pi}{3}}+1+4e^{-i\frac{2\pi}{3}})]+[2u_{xy}\frac{\sqrt{3}}{4}a^2(e^{i\frac{2\pi}{3}}-1)]. \tag{36}$$

Using the fact that

$$e^{i\frac{-2\pi}{3}} + 1 + e^{i\frac{2\pi}{3}} = 0,$$

we get

$$\tilde{\gamma_K} = -\gamma_0 \beta \frac{3}{4}[(u_{xx} - u_{yy})e^{-i\frac{2\pi}{3}} - 2u_{xy}\frac{1}{\sqrt{3}}(e^{i\frac{2\pi}{3}} + 1)]. \tag{37}$$

Realizing that

$$\frac{1}{\sqrt{3}}(e^{i\frac{2\pi}{3}} - 1) = -ie^{-i\frac{2\pi}{3}},$$

we can write $\tilde{\gamma_K}$ as

$$\tilde{\gamma_K} = -\gamma_0 \frac{3}{2}a(A_x - iA_y)e^{-i\frac{2\pi}{3}}, \tag{38}$$

and the full addition to the Hamiltonian due to strain is

$$\tilde{H}^{(K)} = v_F(\sigma \cdot \vec{A})\alpha \tag{39}$$

where

$$\vec{A} = \frac{\beta}{2a}((u_{xx} - u_{yy}), (-2u_{xy})), \tag{40}$$

and

$$\alpha = e^{-i\frac{2\pi}{3}} \tag{41}$$

is the same term that appears in the original Hamiltonian. Similarly for $K' = \frac{2\pi}{3a}(-\frac{1}{\sqrt{3}},1)$, and keeping in mind that

$$\begin{aligned} K' \cdot \delta_1 &= 0 \\ K' \cdot \delta_2 &= \frac{-2\pi}{3} \\ K' \cdot \delta_3 &= \frac{2\pi}{3}, \end{aligned} \tag{42}$$

we get

$$\tilde{\gamma_K'} = -\gamma_0 \frac{3}{2}a(A_x + iA_y)e^{i\frac{2\pi}{3}}, \tag{43}$$

and the strain contribution to the Hamiltonian is

$$\tilde{H}^{(K')} = v_F(\sigma^* \cdot (-\vec{A}))\alpha^* \tag{44}$$

Since again we remove the same term α by a unitary transformation, the Hamiltonian expressed in equation (26), is modified by strain to

$$\hat{H}_g^k \approx v_F \sigma \cdot (\boldsymbol{q} + \boldsymbol{A}), \tag{45}$$

while equation (27) becomes

$$\hat{H}_g^{k'} \approx -v_F \sigma^* \cdot (\boldsymbol{q} - \boldsymbol{A}). \tag{46}$$

From equations (45), and (46) we conclude that strain modifies the Hamiltonian by adding the vector $\vec{A}$ to the K points and $-\vec{A}$ to K' points; aside from the changing signs, $\vec{A}$ resembles the minimal substitution of the electromagnetic vector potential, but since the vector changes sign depending on the valley, it is referred to as pseudo-vector potential.

3.2 Gauge freedom of a general strain field

Similar to the gauge freedom in electromagnetic fields, the pseudo magnetic field resulting from strain in graphene is invariant under certain transformations of the strain field. Since the pseudo-magnetic field is given by

$$B = \vec{\nabla} \times \vec{A}, \tag{47}$$

then adding the gradient of any function Φ to $\vec{A}$ does not change the pseudo-magnetic field, since

$$\vec{\nabla} \times \nabla\Phi = 0. \tag{48}$$

When we use the pseudo-magnetic field to make inferences about the strain in graphene, it should be taken into account that certain forms of strain cannot be detected in this way. We start by assuming the general transformations

$$u_x \longrightarrow u_x + a,$$

$$u_y \longrightarrow u_y + b,$$

where u_x is the x-displacement, and u_y the y-displacement of the atoms at a given position, and a and b are some scalar functions of position. Requiring that a and b leave the pseudo-magnetic field invariant gives the conditions on the freedom of the strain field.

Using the gauge freedom of the pseudo-vector potential, where adding a divergence of a function Φ does not affect the pseudo-magnetic field

$$A_x \longrightarrow A_x + \partial_x \Phi,$$

$$A_y \longrightarrow A_y + \partial_y \Phi,$$

and given that the transformed electromagnetic pseudo-vector due to the transformed strain is

$$A_x = \frac{\beta}{2a}(\partial_x u_x - \partial_y u_y + [\partial_x a - \partial_y b]) \tag{49}$$

$$A_y = -\frac{\beta}{2a}(\partial_x u_y + \partial_x u_y + [\partial_x b + \partial_y a]), \tag{50}$$

we get the conditions

$$\partial_x a - \partial_y b = \partial_x \Phi, \tag{51}$$

$$-\partial_x b - \partial_y a = \partial_y \Phi, \tag{52}$$

for some function $\Phi(x,y)$.

In the following calculation, I assume that the strains in the x and y directions are independent of one another, and so equations (51) and (52) can be solved separately for a and b.

3.2.1 Invariance under u_x transformations

For the u_x component of the strain, equations (51) and (52) are

$$\partial_x \Phi_1 = \partial_x a, \tag{53}$$

and

$$\partial_y \Phi_1 = -\partial_y a. \tag{54}$$

Aplying ∂_y to equation (53), and ∂_x to equation (54) gives

$$\partial_x \partial_y \Phi_1 = \partial_x \partial_y a, \tag{55}$$

and

$$\partial_x \partial_y \Phi_1 = -\partial_x \partial_y a, \tag{56}$$

from (55) and (56) we get

$$\partial_x \partial_y a = 0,$$

which gives the solution for a as

$$a(x,y) = f_1(x) + f_2(y). \tag{57}$$

Therefore, the pseudo-magnetic field is invariant under displacements of atoms in the x-direction which vary in the x or y directions independently.

3.2.2 Invariance under u_y transformations

For the invariance of an independent u_y component, the equations (51) and (52) are reduced to

$$\partial_x \Phi_2 = -\partial_y b, \tag{58}$$

and

$$\partial_y \Phi_2 = -\partial_x b. \tag{59}$$

Applying ∂_y to both sides of equation (58), and ∂_x to both sides of (59) gives

$$\partial_y \partial_x \Phi_2 = -\partial_y \partial_y b, \tag{60}$$

and

$$\partial_y \partial_x \Phi_2 = -\partial_x \partial_x b. \tag{61}$$

Therefore, from equations (60) and (61), we get

$$\partial_y \partial_y b = \partial_x \partial_x b. \tag{62}$$

Writing b in terms of its Fourier transformation

$$b = \int e^{-i(kx+qy)} \tilde{b}(k,q) dk dq,$$

and from equation (62) we get that

$$k = \pm q,$$

so

$$b = \int e^{-ik(x+y)}\tilde{b}(k)dk + \int e^{-ik(x-y)}\tilde{b}(k)dk.$$

This means that b is an arbitrary function of $(x+y)$ or $(x-y)$, so we write the general form of b similar to equation (57) as

$$b(x,y) = g_1(x+y) + g_2(x-y). \tag{63}$$

Therefore the Hamiltonian is invariant under displacements of atoms in the y-direction which vary in the $x+y$ or $x-y$ directions independently.

3.2.3 Invariant strain fields

From equations (57) and (63), we conclude that a strain field where the displacement in the x direction is independent along lines parallel to the x and y axes, while displacement in the y direction is the same along the lines $x+y=c$ and $x-y=c$ for any constant c. Figure 3 below shows such lines of equal strain for the strain field leaving the pseudo-magnetic field invariant. In addition, it is clear that strain fields where $u_{xx} = u_{yy}$ and $u_{xy} = 0$ amount to a volume change of the graphene sheet but does not produce a pseudo-magnetic field.

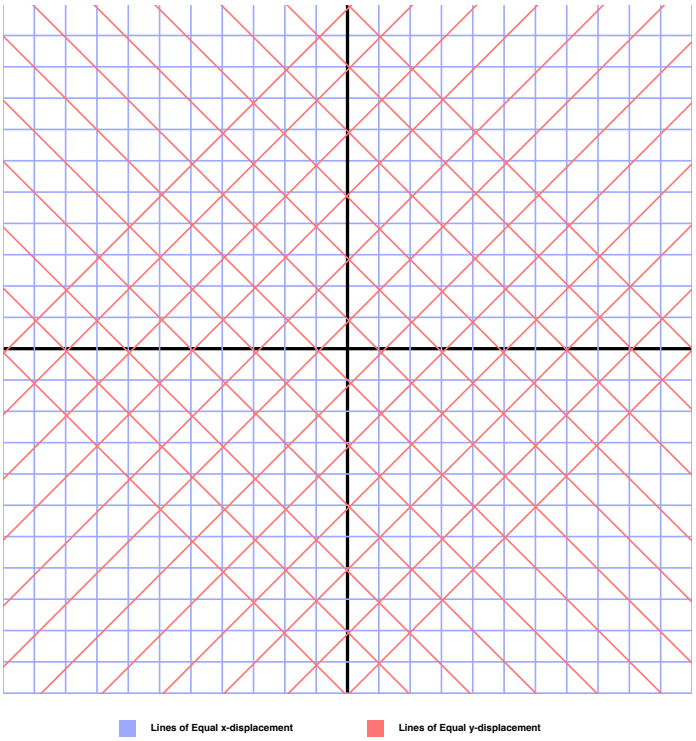

Figure 3. Lines showing the "lines of equal displacement" of the x and y strain vectors for a strain field leaving the pseudo-magnetic field invariant

4 Periodic strain

4.1 Periodic strain in Graphene

Periodic strain can arise in graphene due to the mismatch between the graphene lattice and the substrate lattice [11]. In addition, patterns of periodic strain may also appear in optical forging experiments as a concentrated laser beam creates ripples in the graphene sheet [12]. In the following discussion, the optical response of periodically strained graphene is studied by adding the strain as an electromagnetic vector according to equation (44) to the Hamiltonian obtained in (26). We begin by assuming a displacement vector in the y-direction which is periodic in x. In what follows we assume that the period of the strain is much larger than the graphene lattice constant, which allows us to ignore the periodicity of the variables q_x, and q_y in unstrained graphene, and consider the Hamiltonian as a periodic function in x only.

The strain field

$$u = (0, \beta' \sin \frac{2\pi x}{L}), \tag{64}$$

is periodic in the x-direction with period L with amplitude β, and it results in the pseudo-magnetic vector potential

$$A = (0, -\frac{2\pi\beta'}{L} \cos \frac{2\pi x}{L}).$$

For simplicity we define $\beta = 2\pi\beta'$

$$A = (0, -\frac{\beta}{L} \cos \frac{2\pi x}{L}). \tag{65}$$

With the pseudo-magnetic vector potential (65), we get the Hamiltonian

$$H = v_F \int dx[\hat{q}_x\sigma_x + \hat{q}_y\sigma_y + \frac{\beta}{L} \cos(\frac{2\pi x}{L})\sigma_y], \tag{66}$$

With the limit of continuous momenta and periodic strain given in equation (66), the Hamiltonian is periodic in the x-direction with period L. In the next section, I use Bloch's theorem to simplify the Hamiltonian above for use in calculations.

4.2 Bloch's theorem for supercells

Given the periodicity of the strain, we can use Bloch's theorem to write the full wave function in the form

$$\psi_k(r) = \sum_{G_n} C(G_n) e^{i(q_x+G_n)x} e^{i(q_y y)}, \tag{67}$$

where $G_n = \frac{2\pi n}{L}$. The Hamiltonian in equation (66) can be written in the same basis as (67) to give

$$H(k) = v_F \sum_{G_n} [(q_x + G_n)\sigma_x + q_y \sigma_y]\delta_{m,n} + \frac{\beta\sigma_y}{2L}[\delta_{m,n+1} + \delta_{m,n-1}], \tag{68}$$

The result in equation (68) expresses the Hamiltonian in terms of an infinite matrix with the first term giving the diagonal components and the second for off-diagonal components. The off-diagonal components represent the coupling between different super-cells in momentum space, which couples each cell m to neighboring cells $m \pm 1$. In what follows, I solve the spectrum of equation (68) numerically. In the numerics I use only a finite number of components as the coupling with further cells becomes less and less important.

5 Optical properties

5.1 Optical conductivity

In this section I calculate the optical conductivity in graphene by considering a small perturbation which represents electromagnetic radiation. The section follows the derivation in Katsnelson's textbook [9].

Let

$$H = H_0 + V. \tag{69}$$

Here V is a small perturbation depending on time as

$$V(r,t) = V(r)e^{-i\omega t+\delta t}$$

where $\delta > 0$ is infinitesimally small. Then the change in the density matrix elements due to V is

$$\delta\rho'_{nm} = \frac{f_n - f_m}{E_m - E_n - (\omega + i\delta)}V_{nm}, \tag{70}$$

where $f_i = f(E_i)$ is the Fermi function of the i^{th} energy level, and $V_{nm} = \langle m| V |m\rangle$. A perturbation on the expectation value of an observable A is $\delta A e^{-i\omega t+\delta t}$ where

$$\langle \delta A\rangle = \mathrm{Tr}\Big\{A\rho'\Big\} = \sum_{m,n}\frac{f_n - f_m}{E_m - E_n - (\omega + i\delta)}V_{nm}A_{mn}. \tag{71}$$

Considering the perturbation due to an oscillating electric field which represents the incident light, the potential is given by

$$V = \vec{r}\cdot\vec{E} \tag{72}$$

where we use natural units in which the electron charge $e = 1$. Here $\vec{E} = Ee^{-i\omega t+\delta t}$, and r is the position vector, which is expressed in the momentum space as

$$\vec{r} = i\vec{\nabla}_k. \tag{73}$$

The current operator is defined as the electric charge multiplied by the time-derivative of the position operator, which can be evaluated by the Heisenberg equation of mo-

tion to give [9]

$$\vec{j} = e\frac{d\vec{r}}{dt} = ie[\hat{H}, \hat{r}], \tag{74}$$

and the conductivity is defined as

$$\sigma_{\alpha\beta} = \frac{j_\alpha}{E_\beta}. \tag{75}$$

Using equations (71) and (75), the conductivity can be defined as

$$\sigma_{\alpha\beta} = \sum_{m,n} \frac{f_n - f_m}{E_m - E_n - (\omega + i\delta)} \langle n| r_\beta |m\rangle \langle m| j_\alpha |n\rangle . \tag{76}$$

Using the definition of j in equation (74), we get

$$\langle m| j_\alpha |n\rangle = i \langle m| [H,r_\alpha] |n\rangle = i(E_m - E_n) \langle m| r_\alpha |n\rangle .$$

Therefore we can write the position matrix element as

$$\langle m| r_\alpha |n\rangle = -i\frac{\langle m| j_\alpha |n\rangle}{(E_m - E_n)}. \tag{77}$$

Then substituting (77) in (76) gives

$$\sigma_{\alpha\beta} = -i \sum_{m,n} \frac{f_n - f_m}{E_m - E_n + (\omega + i\delta)} \frac{1}{E_m - E_n} \langle n| j_\beta |m\rangle \langle m| j_\alpha |n\rangle , \tag{78}$$

and we finally get the equation for the diagonal component of optical conductivity

$$\sigma_{xx} = -i \sum_{m,n} \frac{f_n - f_m}{E_m - E_n - (\omega + i\delta)} \frac{1}{E_m - E_n} |\langle n| j_x |m\rangle|^2.$$

Since $j_x = v_F \sigma_x$ in graphene [9],we get

$$\sigma_{xx} = -iv_F^2 \sum_{m,n} \frac{f_n - f_m}{E_m - E_n - (\omega + i\delta)} \frac{1}{E_m - E_n} |\langle n| \sigma_x |m\rangle|^2. \tag{79}$$

It is possible now to calculate the optical conductivity for graphene by diagonalising the Hamiltonian given in equation (68), and substituting its eigenenergies and eigenstates in (79).

5.2 Reflectivity

In this section, I calculate the reflectivity of a graphene sheet as a function of its optical conductivity. To calculate the reflectivity, I write the Maxwell's equations for a plane-wave electromagnetic radiation crossing perpendicularly to the graphene sheet suspended in vacuum as shown in figure 4. The following calculation expands the results given in [13] to consider different angles of incidence.

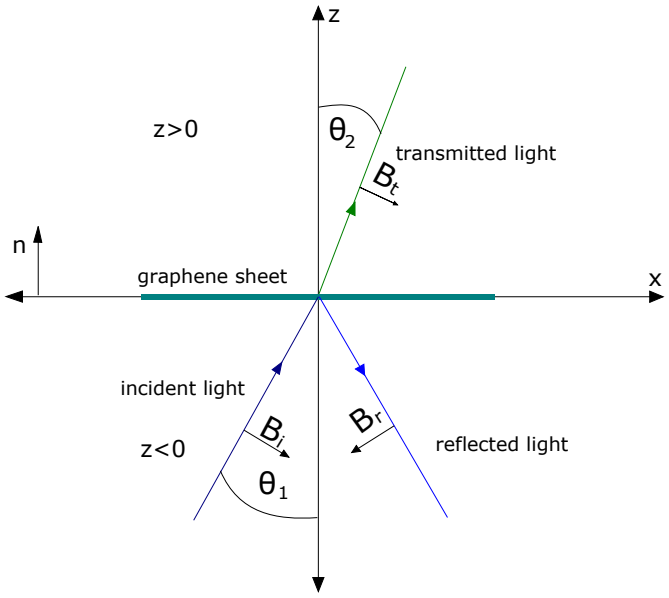

Figure 4. Light incident over graphene sheet

Assuming the light has s-polarisation and setting the electric field in the y-direction, the boundary conditions at $z = 0$ are

$$n \times (E^1 - E^2) = 0, \tag{80}$$

and

$$n \times (B^1 - B^2) = \mu_0 j, \tag{81}$$

where E^1, B^1, are the fields in $z < 0$, while E^2, B^2 are the fields in $z > 0$, n is the unit vector in the z direction, μ_0 is the vacuum permeability, and j is the electric current. The boundary conditions can be written in components as

$$E^i - E^r = E^t, \tag{82}$$

where E^i, E^r, and E^t are the incident, reflected and transmitted electric fields respectively, and

$$(B^i + B^r)\cos\theta_1 = B^t \cos\theta_2 + \mu_0 \sigma E^t, \tag{83}$$

where B^i, B^r, and B^t are the incident, reflected and transmitted magnetic fields respectively. In the last step we used equation (75). The Faraday equation in component form at $z > 0$ is

$$\begin{aligned} -\partial_z E_y^t &= -\partial_t B_x^t \\ \partial_x E_y^t &= -\partial_t B_z^t, \end{aligned} \tag{84}$$

which, for plane waves, becomes

$$\begin{aligned} -E_y^t k_z &= -\omega B_x^t \\ E_y^t k_x &= -\omega B_z^t. \end{aligned} \tag{85}$$

Since $\omega^2 = (k_x^2 + k_z^2) = k^2$ and $|E^t| = E_y^t$, we get

$$\left|E^t\right| = \left|B^t\right|, \tag{86}$$

while for $z < 0$ we have

$$\begin{aligned} -k_z(E_y^i + E_y^r) &= -\omega(B_x^i + B_x^r) \\ k_x(E_y^i + E_y^r) &= -\omega(B_z^i + B_z^r), \end{aligned} \tag{87}$$

from which we get

$$\left|E^i + E^r\right| = \left|B^i + B^r\right|. \tag{88}$$

Using equations (86) and (88), equation (83) is written as

$$(E^i + E^r)\cos\theta_1 = (\mu_0\sigma(\omega) + \cos\theta_2)E^t, \tag{89}$$

using equation (82), this becomes

$$2E^r\cos\theta_1 = [\frac{\sigma(\omega)}{\epsilon_0} + \cos\theta_2 - \cos\theta_1]E^t, \tag{90}$$

where in the last step we used that $k = \omega$, and $\mu_0 = \frac{1}{\epsilon_0}$. We now write the reflected electric field as

$$E^r = \frac{\frac{\sigma(\omega)}{\epsilon_0} + \cos\theta_2 - \cos\theta_1}{2\cos\theta_1}E^t, \tag{91}$$

which means that the incident field is given by

$$E^i = \frac{\frac{\sigma(\omega)}{\epsilon_0} + \cos\theta_2 + \cos\theta_1}{2\cos\theta_1}E^t. \tag{92}$$

The reflectivity, which is defined as

$$R = \frac{|E^r|^2}{|E^i|^2} \tag{93}$$

is given by

$$R = \frac{|\sigma(\omega) + \epsilon_0(\cos\theta_2 - \cos\theta_1)|^2}{|\sigma(\omega) + \epsilon_0(\cos\theta_2 + \cos\theta_1)|^2}. \tag{94}$$

Here $\epsilon_0 = \frac{\alpha}{4\pi} \approx \frac{137}{4\pi}$, where α is the fine structure constant, since we set $e = c = \hbar = 1$.

When the media on both sides of the sheet are vacuum, we can set $\theta_1 = \theta_2 \equiv \theta$, and we get the result

$$R = \frac{|\sigma(\omega)|^2}{|\sigma(\omega) + 2\epsilon_0(\cos\theta)|^2}. \tag{95}$$

Similarly for p-polarisation, the reflectivity of graphene suspended in vacuum is given by

$$R = \frac{|\sigma(\omega)|^2}{|\sigma(\omega) + 2\epsilon_0|^2}. \tag{96}$$

Using equations (79), (95), and (96), we can calculate the conductivity and reflectivity of strained graphene suspended in vacuum.

5.3 Conductivity and reflectivity of pristine graphene

Equation (79) should give the value of optical conductivity for pristine (i.e. non-strained) graphene; in this section I confirm that substituting the eigenvalues and eigenstates given in equations (28), (29), and (29) into (79) gives the value for optical conductivity for pristine graphene given in the literature, then I substitute that value into equation (95) to calculate the reflectivity of pristine graphene. For pristine graphene, we have for each momentum vector a hole-state and electron-state with energies

$$E_{n,m} = \pm v_F q,$$

and to simplify we can calculate here the last term of equation (79) in the K valley as

$$\begin{aligned} |\langle n|\sigma_x|m\rangle|^2 &= |\frac{1}{\sqrt{2}}\begin{pmatrix} e^{-i\frac{\theta}{2}} \\ e^{i\frac{\theta}{2}} \end{pmatrix}\sigma_x \frac{1}{\sqrt{2}}\begin{pmatrix} e^{i\frac{\theta}{2}} & -e^{-i\frac{\theta}{2}} \end{pmatrix}|^2 \\ &= [\frac{1}{2}(-e^{-i\theta}+e^{i\theta})]^2 \\ &= \sin^2\theta, \end{aligned}$$

where the same result also applies for states in the K' valley. Then we substitute this into (79) and get

$$\begin{aligned} \sigma_{xx} &= -iv_F^2 \int \frac{dqd\theta}{(2\pi)^2} q \frac{1}{(2E-\omega)-i\delta}\frac{1}{2E}|\langle n|\sigma_x|m\rangle|^2 \\ &= v_F^2 \int \frac{dqd\theta}{(2\pi)^2} q \frac{\delta - i(2E-\omega)}{(2E-\omega)^2+\delta^2}\frac{1}{2E}\sin^2\theta. \end{aligned}$$

Taking $\delta \longrightarrow +0$, and noting that

$$\frac{\delta}{(2E-\omega)^2+\delta^2} \longrightarrow \pi\delta(2E-\omega) \tag{97}$$

we get

$$\mathrm{Re}\{\sigma_{xx}\} = \pi v_F^2 \int \frac{dqd\theta}{(2\pi)^2} q\delta(2E-\omega)\frac{1}{2E}\sin^2\theta. \tag{98}$$

We can now perform the change of variables

$$\begin{aligned} q &= \frac{E}{v_F} \\ dq &= \frac{dE}{v_F}, \end{aligned}$$

to find

$$\begin{aligned}\mathrm{Re}\{\sigma_{xx}\} =& \frac{v_F^2\pi}{4\pi^2 v_F^2}\int dE d\theta \delta(2E-\omega)\frac{E}{2E}\sin^2\theta \\ =& \frac{1}{8\pi}\int dE d\theta \delta(2E-\omega)\sin^2\theta \\ =& \frac{1}{8\pi}\int d\theta \sin^2\theta = \frac{1}{8}\end{aligned}$$

Multiplying by 2 to account for both valleys gives the final result

$$\mathrm{Re}\{\sigma_{xx}\} = \frac{1}{4} = \sigma_0, \tag{99}$$

which agrees with the known results for pristine graphene [4], [9]. Using the result from (99), and given that in the chosen system of natural units we have $\epsilon_0 = \frac{1}{4\pi\alpha}\frac{e^2}{\hbar} = \frac{1}{4\pi\alpha}$, we get the reflectivity for perpendicular light

$$R = \frac{|\frac{1}{4}|^2}{|\frac{1}{4}+\frac{1}{2\pi\alpha}|^2}. \tag{100}$$

It is simplified to

$$R = \frac{|\frac{1}{2}\pi\alpha|^2}{|\frac{1}{2}\pi\alpha+1|^2} = \frac{\frac{1}{4}\pi^2\alpha^2}{(\frac{1}{2}\pi\alpha+1)^2}, \tag{101}$$

which agrees with the known result for the reflectivity of graphene [4]. In the following section, the same results are calculated numerically in order to confirm the validity of other calculations that include strain with different amplitudes added to the Hamiltonian.

6 Calculations

6.1 Numerical methods

6.1.1 Energy scale

The Hamiltonian in equation (68) can be written in terms of dimensionless variables with the prefactor $\frac{v_F}{2L}$, so that the matrix itself does not depend on the period of the strain, and the calculation remains independent of the energy scale. This allows for considering the energy scale and different periods of the strain after the calculation, rather than needlessly complicating calculations with an additional variable parameter (namely L). The Hamiltonian thus becomes

$$H(k) = \frac{v_F}{2L} \sum_{G_n} [(\tilde{q}_x + \tilde{G}_n)\sigma_x + \tilde{q}_y \sigma_y]\delta_{m,n} + \beta\sigma_y[\delta_{m,n+1} + \delta_{m,n-1}], \tag{102}$$

where

$$\begin{aligned} \tilde{q} &= q * 2L \\ \tilde{G}_n &= 4\pi n \end{aligned} \tag{103}$$

are dimensionless variables. Similarly I define the dimensionless variables

$$\begin{aligned} \tilde{E} &= E\frac{2L}{v_F} \\ \tilde{T} &= T\frac{2L}{v_F} \\ \tilde{\omega} &= \omega\frac{2L}{v_F}. \end{aligned} \tag{104}$$

Now, equation (79) can be expressed in the form

$$\sigma_{xx}(\tilde{\omega}) = -i \sum_{m,n} \int \frac{d\tilde{q_x} d\tilde{q_y}}{(2\pi)^2} \frac{1}{\tilde{E}_m - \tilde{E}_n - (\tilde{\omega} + i\delta)} \frac{f_n - f_m}{\tilde{E}_m - \tilde{E}_n} |\langle n| \sigma_x |m\rangle|^2, \tag{105}$$

where the $\tilde{q_x}$ integral is over one momentum-space super-cell. Equation (105) shows that for the calculation of the optical conductivity, the energy scale only shows in re-scaling the frequency.

6.1.2 Momentum valleys

Equation (102) only includes one momentum valley, but to find the value of σ_{xx} from equation (105), we need to sum $\sigma_{xx}^{(K)}$ and $\sigma_{xx}^{(K')}$. However, the fact that

$$H^{(K)} = -H^{*(K')}, \tag{106}$$

implies that

$$\sigma_{xx}^{(K)} = \sigma_{xx}^{(K)}, \tag{107}$$

and the result is simply

$$\sigma_{xx} = 2\sigma_{xx}^{(K)}. \tag{108}$$

This analytical result is also confirmed numerically by finding the eigenvalues and eigenstates for both momentum valleys, and ensuring that

$$\begin{aligned} \psi_n^{(K)} - \psi_n^{(K')^*} &= 0, \\ \tilde{E}_n^{(K')} + \tilde{E}_n^{(K')} &= 0, \end{aligned} \tag{109}$$

hold for different values of β. The numerical checks confirmed that this is true for all values of β included.

6.1.3 Parameters

The main free parameters to be selected for the calculation are the energy level cutoff corresponding to the number of elements to include from the infinite sum in equation (102), the momentum cutoff which correspond to the $d\tilde{q}_y$ integral limits in equation (105), and the energy levels m,n to include in the sum in (105) .

- **Momentum cutoff and energy levels to sum over**

  The y-momentum cutoff and the energy levels n,m in equation (105) are related to the frequencies of the incident light; since the conservation of energy implies that the energy difference $\tilde{E}_m - \tilde{E}_n$ does not exceed the highest energy of the incident photons $\tilde{\omega}$, then given the maximum frequency $\tilde{\omega}_{\max}$, we may select $\tilde{q}_y \in [-\frac{1}{2}\tilde{\omega}_{\max}, \frac{1}{2}\tilde{\omega}_{\max}]$, while the highest energy level m to include in the sum could be selected such that $\tilde{E}_m(\tilde{q}_y = 0) - \tilde{E}_{-m}(\tilde{q}_y = 0) = \tilde{\omega}_{\max}$. Figure 5 shows the energy as a function of $\tilde{q}_y$ with $\tilde{q}_x = 0$ for different values of β, while figure 6 shows the energy as a function of $\tilde{q}_x$ with $\tilde{q}_y = 0$ for the first two levels (i.e. m,$n = 0, \pm 1$) for different values of β.

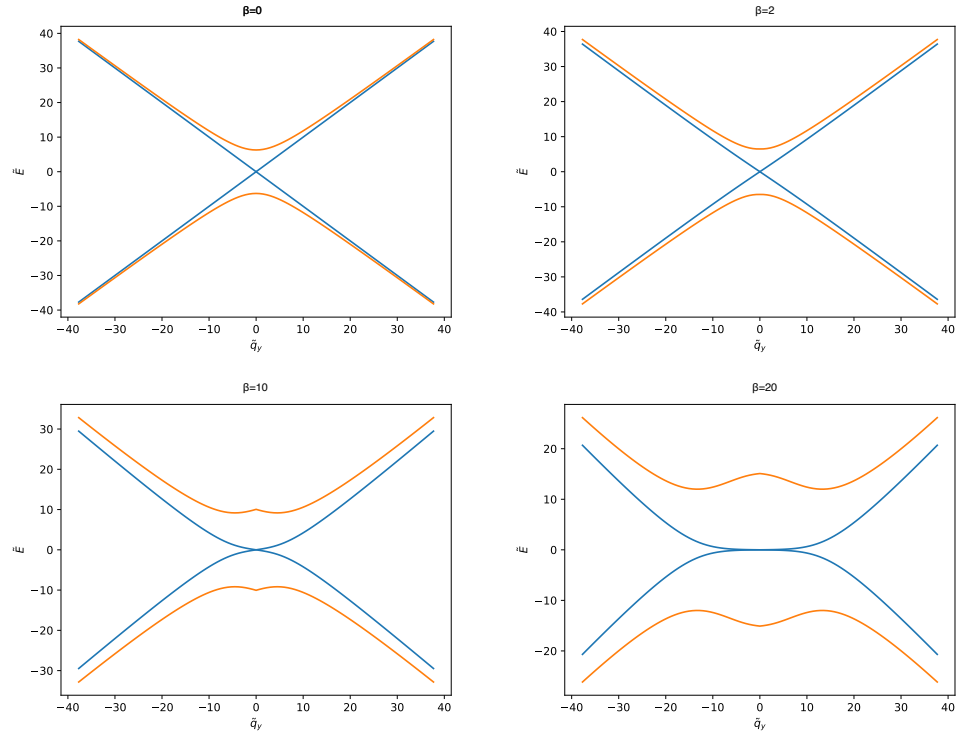

Figure 5. Plot of $\tilde{E}$ as a function of $\tilde{q}_y$ at $\tilde{q}_x = 0$ for energy levels $n = 0, \pm 1$

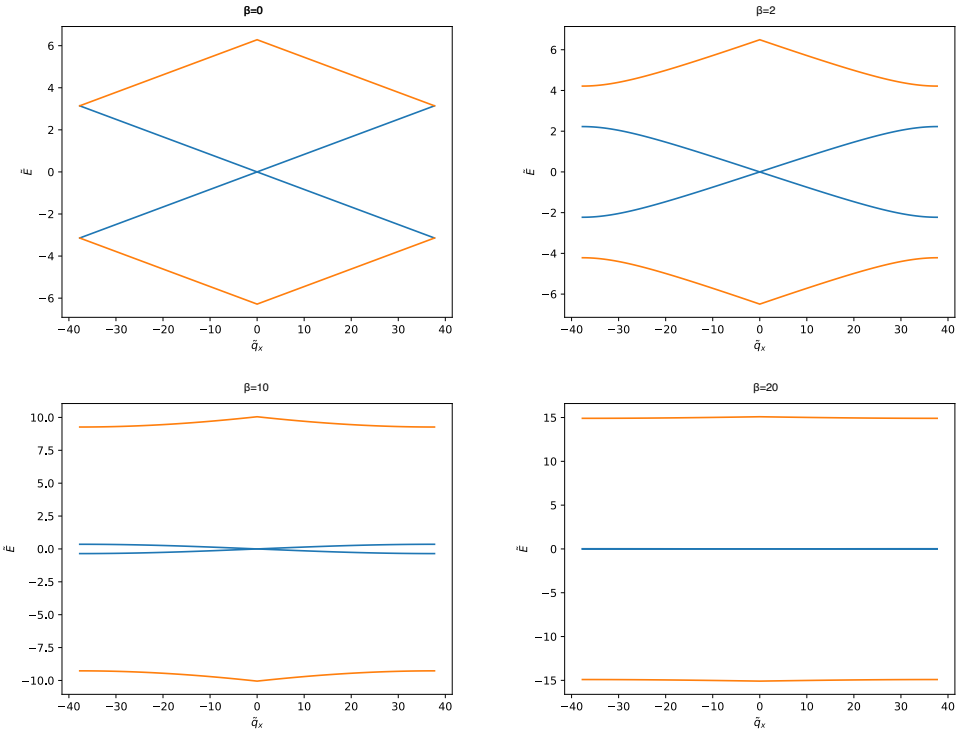

Figure 6. Plot of $\tilde{E}$ as a function of $\tilde{q}_x$ at $\tilde{q}_y = 0$ for energy levels $n = 0, \pm 1$

The plots indicate that for $\tilde{\omega}_{\max} = 20$, $\tilde{q}_y \in [-40,40]$ should cover the energy differences of interest up to $\beta = 20$, and I have selected these values for the integral. I have also selected $n,m \in 0, \pm 1, \pm 2, \pm 3, \pm 4, \pm 5$.

- **Hamiltonian matrix elements**

  Since the Hamiltonian given in equation (102) has an infinite number of elements as $m,n = 0, \pm 1, \pm 2,..$, a cutoff N such that $m,n = 0, \pm 1, \pm 2,.. \pm N$ must be chosen before it can be used numerically. To select the correct cutoff, I have calculated the expected improvement in accuracy from adding one more term by finding the difference the eigenvalues from cutoffs N and $N+1$. The change in energy by increasing the cutoff is denoted $\delta\tilde{E}$, and I define it as the average energy difference between corresponding energy levels $i = \pm 1, \pm 2,.. \pm 5$ which is maximized with respect to momentum.

$$\delta\tilde{E} = \tilde{E}(N+1,i) - \tilde{E}(N,i). \tag{110}$$

  Figure 7 shows $\delta\tilde{E}$ for values of $N = 5,6,7,8,9,10$ at different strain amplitudes β. As expected, the value goes to zero as β diminishes, but for higher values of β, $N = 8$ appears to be the optimal value where an increase in N does not significantly improve the accuracy.

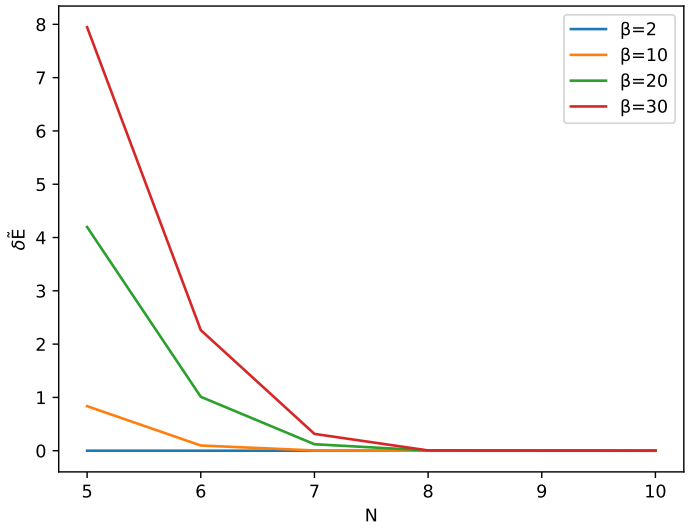

Figure 7. Improved accuracy for increasing the energy cutoff for each N

- **Low energy limit**

  Equation (105) implies that as $\tilde{q}_x, \tilde{q}_y \longrightarrow 0$, the term $\frac{1}{\tilde{E}_m - \tilde{E}_n} \longrightarrow \infty$, which dominates for higher values of β due to the bands flattening. To avoid infinities coming up in calculations for higher values of β, I have used two approaches independently and checked that they give matching results, and that for pristine graphene σ_{xx} approaches σ_0.

  The first approach is to set a minimum value for the frequency (e.g $\tilde{\omega}_{\text{min}} = 2.5$), so that transitions with low energy are not significant, and terms with energy difference below a certain threshold can be ignored (e.g ignore terms with $\tilde{E}_m - \tilde{E}_n < \Delta E_{\text{min}} = 0.1$).

  The second approach is to assume a finite temperature ($\tilde{T} = \Delta E_{\text{min}}$ used above) that is sufficiently small to give similar results to the zero-temperature case, but where the Fermi function can be continuous, and we can replace the expression

$$\frac{f_n - f_m}{\tilde{E}_m - \tilde{E}_n} \xrightarrow{\tilde{E}_m - \tilde{E}_n < E_{\text{min}}} -\frac{\partial f}{\partial \tilde{E}}(\tilde{E}_m) \tag{111}$$

  which is finite at non-zero temperatures. Figure 8 shows that for both approaches σ_{xx} approaches σ_0 for pristine graphene as expected, and they give the same results. The same is true for $\beta \neq 0$, as the figures show below; figure 9 shows the agreement of the results from both methods for $\beta = 2$, and 5, while figures 10, and 11 shows that the results of the two approaches can diverge for higher β, but converge again as $\tilde{T}$, and E_{min} have smaller values.

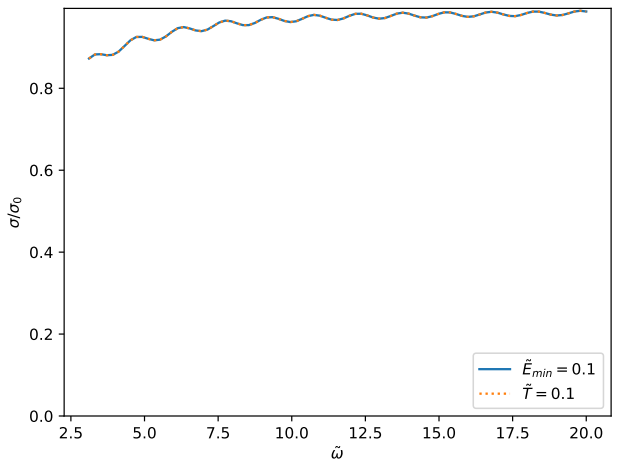

Figure 8. Optical conductivity calculated using both approaches for pristine graphene

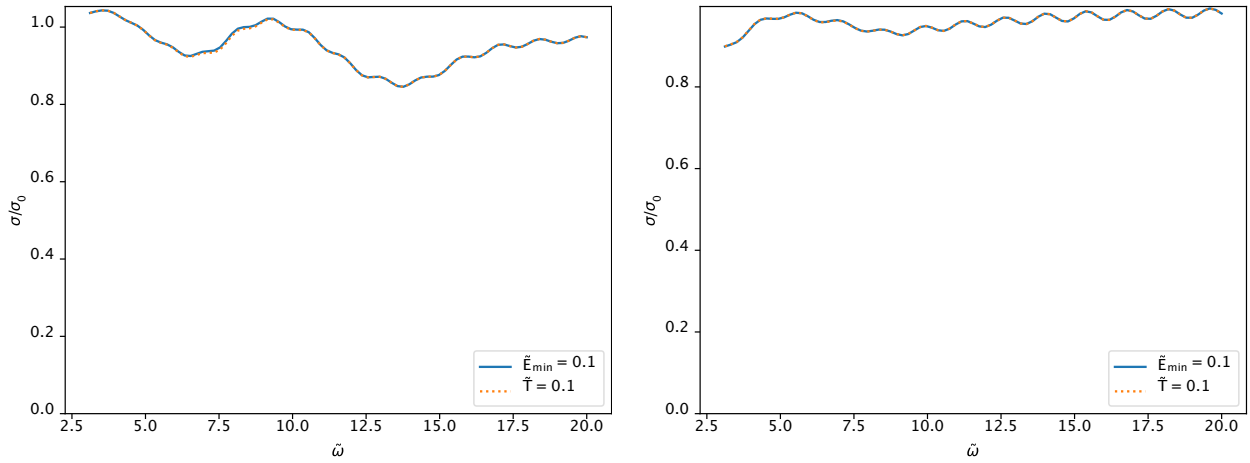

Figure 9. Optical conductivity calculated using both approaches for $\beta = 5$ (left), and $\beta = 2$ (right)

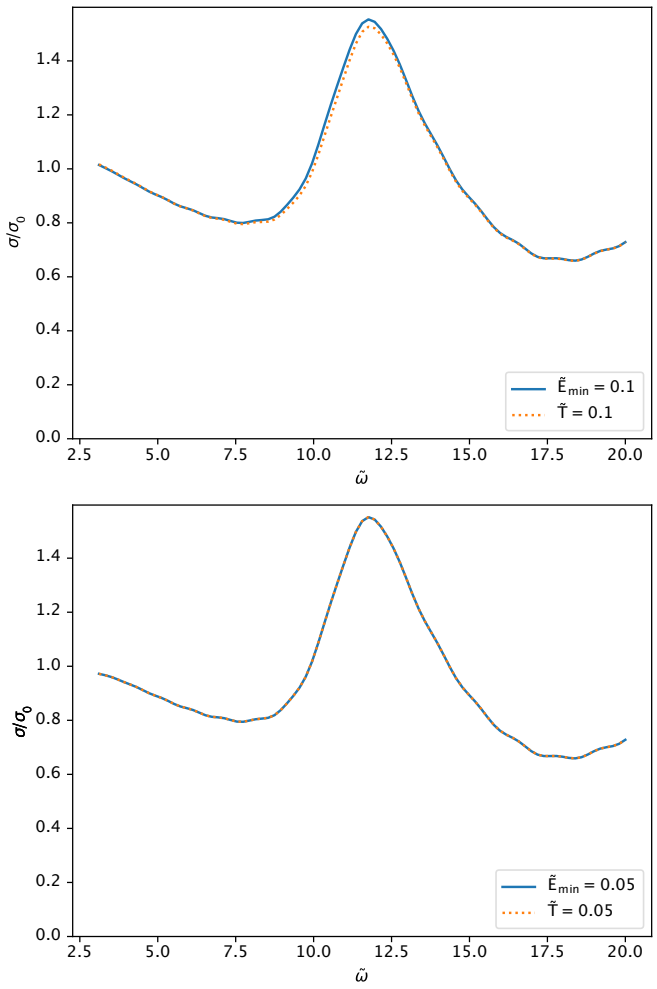

Figure 10. Optical conductivity calculated using both approaches for $\beta = 10$ at $\tilde{E}_{\min} = \tilde{T} = 0.1$ (top) and $\tilde{E}_{\min} = \tilde{T} = 0.05$ (bottom)

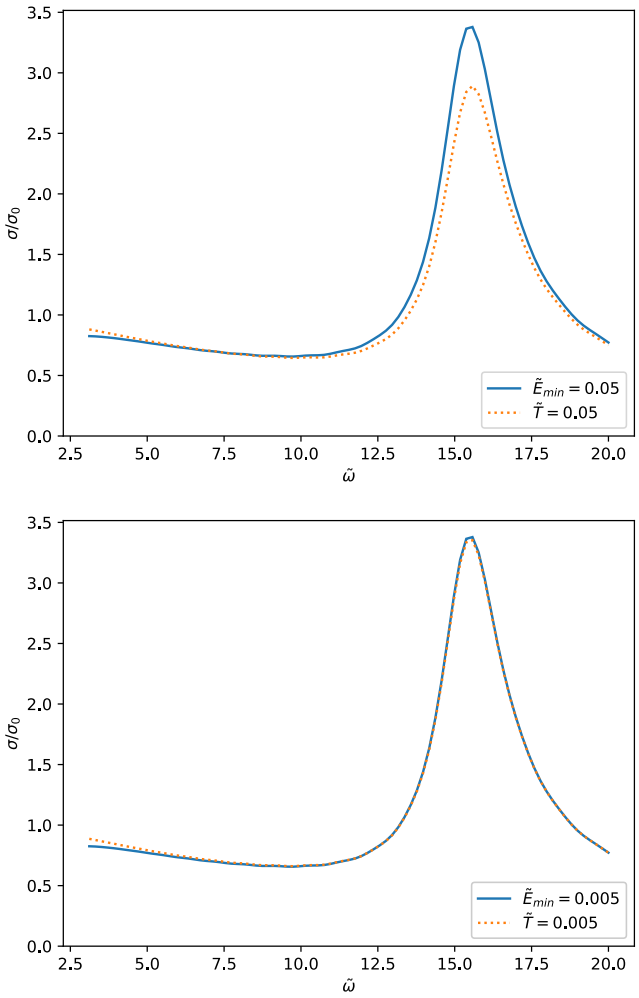

Figure 11. Optical conductivity calculated using both approaches for $\beta = 20$ at $\tilde{E}_{\min} = \tilde{T} = 0.05$ (top) and $\tilde{E}_{\min} = \tilde{T} = 0.005$ (bottom)

6.2 Results

6.2.1 Conductivity

First, I calculated the conductivity of pristine graphene and compared it with the known value of σ_0 [13] [9]. Figure 12 shows σ_{xx}/σ_0 for pristine graphene (i.e. at $\beta = 0$). Note that the comparison is only for the real value of σ_{xx}, since this is the value to which the known value of σ_0 refers [9].

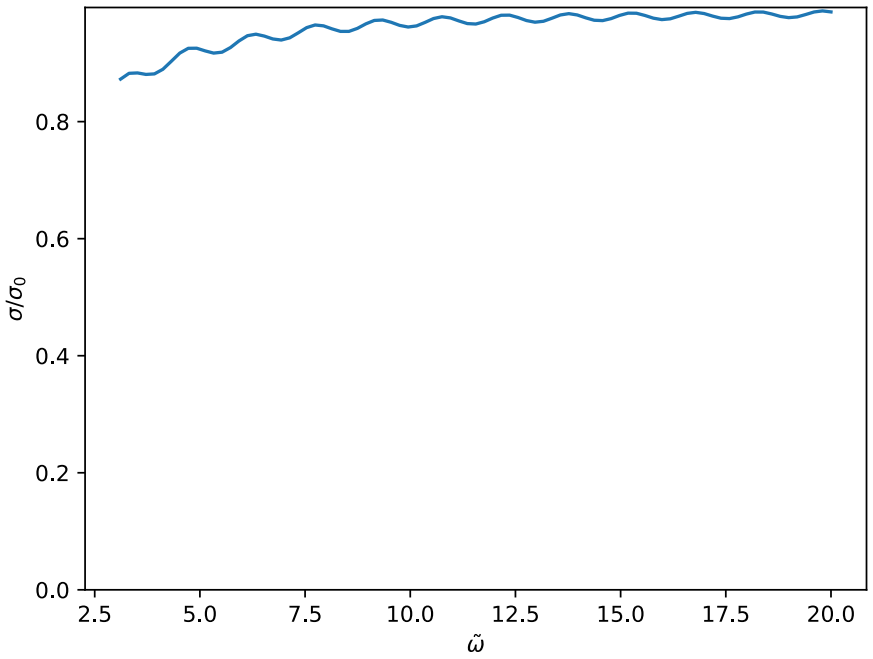

Figure 12. Optical conductivity calculated for bare graphene.

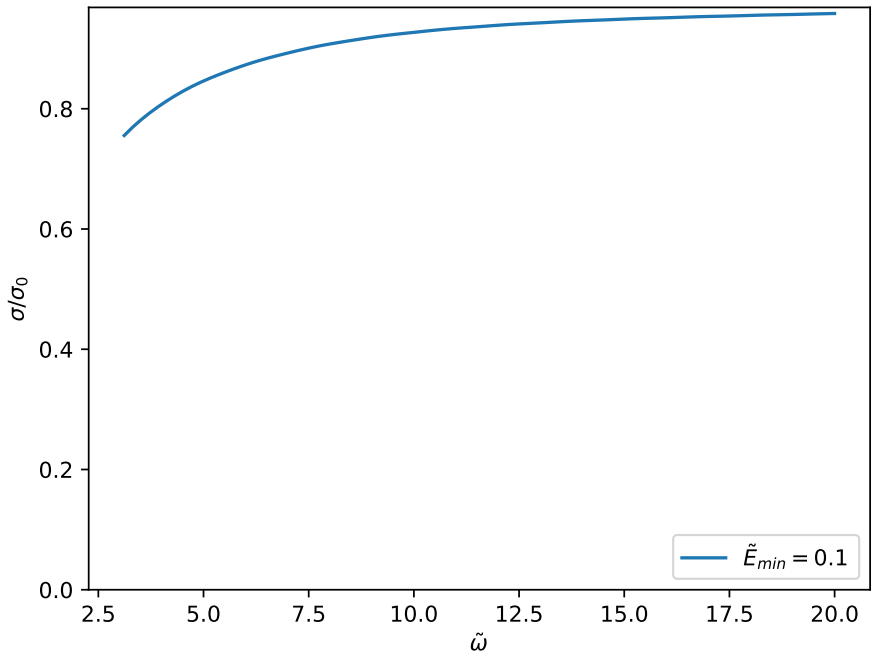

Figure 13. Optical conductivity calculated for bare graphene with higher momentum resolution compared to δ.

Then, I calculate the conductivity for strained graphene with different values of β shown in figure 14. At low values of $\tilde{\omega}$, the conductivity of bare graphene is lower than σ_0, but that effect should be expected for non-zero temperature [13]. The effect of temperature is confirmed in my calculations as shown in the results in figure 15. In the case of zero temperature, a similar effect is caused by ignoring low energy transitions, which can affect the result for low values of $\tilde{\omega}$ due to the inaccuracy involved in the frequency represented by the complex component δ.

It should be noted that part of the inaccuracies at $\tilde{\omega}$ close to zero, as well as the oscillation of the value of σ_{xx} for low values of β are numerical artifacts, possibly due to the ignoring of low-energy transitions and the discretization of the momentum respectively. The latter point is confirmed by calculating the conductivity for bare graphene at different momentum resolutions and corresponding values of the imaginary component of frequency δ; as shown in figure 13, the oscillations disappear when Δq is sufficiently smaller than δ. Finally, the fact that the value of σ_{xx}/σ_0 approaches 1, but is not exactly 1 is due to the various approximations taken, especially taking a cutoff N for energy and limiting the energy levels to sum over, as described in the parameters section above.

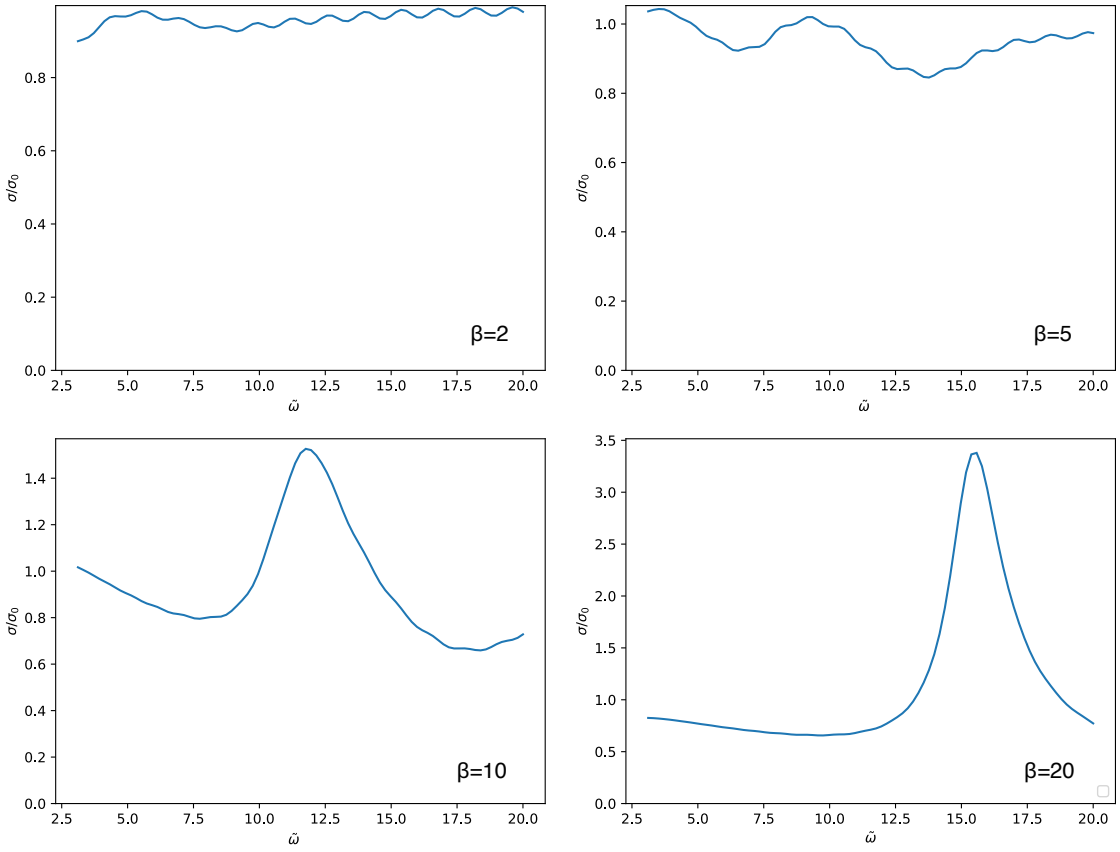

Figure 14. Optical conductivity calculated for strained graphene at different amplitude of strain β

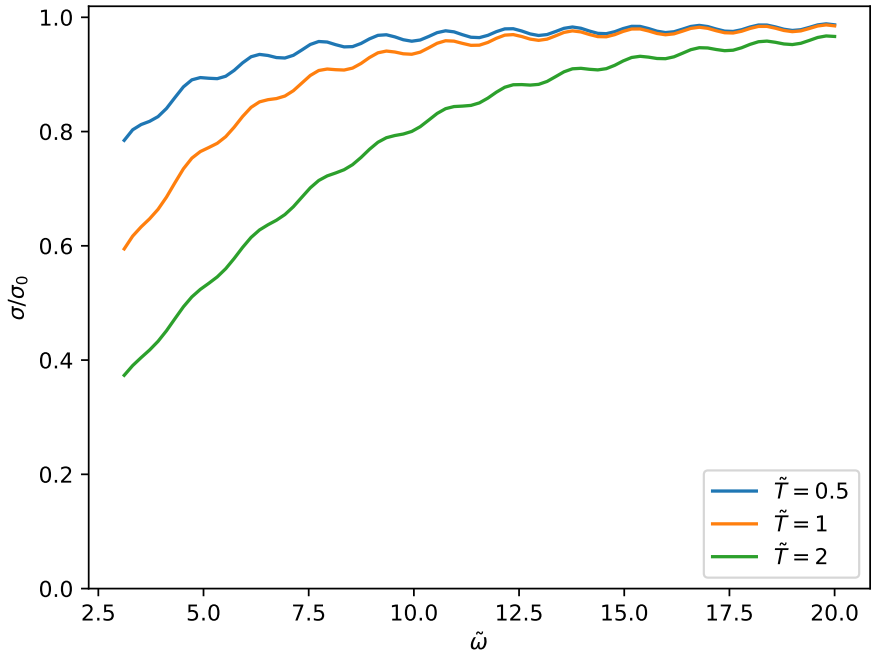

Figure 15. Optical conductivity for bare graphene at different temperatures.

The results also show similar behaviour of σ_{xx} at lower values of β, while the deviation from bare graphene appears to be continuous as the strain increases.

6.2.2 Reflectivity

Given the conductivity, the reflectivity can be calculated directly from equation (95). However, to get results that correspond to real values of frequency, values of the strain period L must be assumed. Figure 16 shows reflectivity of bare graphene as a function of $\tilde{\omega}$ for perpendicular light (θ=0). The result should be compared with the value in equation (101) which has $R \approx 1.310^{-4}$. The calculated reflectivity approaches that value as $\tilde{\omega}$ increases, however at lower frequencies the imaginary component of the conductivity is higher, leading to a higher reflectivity.

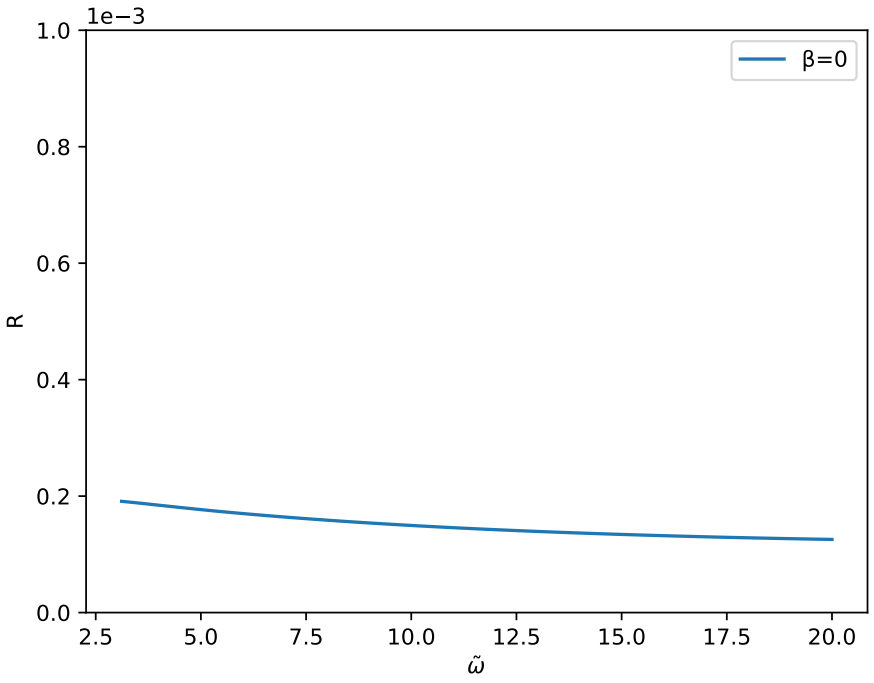

Figure 16. Reflectivity of bare graphene.

Figure 17 shows the same result for weakly strained graphene ($\beta = 2$), which shows only a small deviation from the reflectivity of bare graphene. Figure 18 shows the reflectivity of strained graphene for values of β = 5,10, and 20, for perpendicular light. Finally, figure 19 shows the reflectivity for graphene strained at $\beta = 20$ for different angles of incident light with s-polarisation. Since $\omega = \tilde{\omega} * \frac{v_F}{2L}$, changing the strain period amounts only to re-scaling the x-axis for reflectivity.

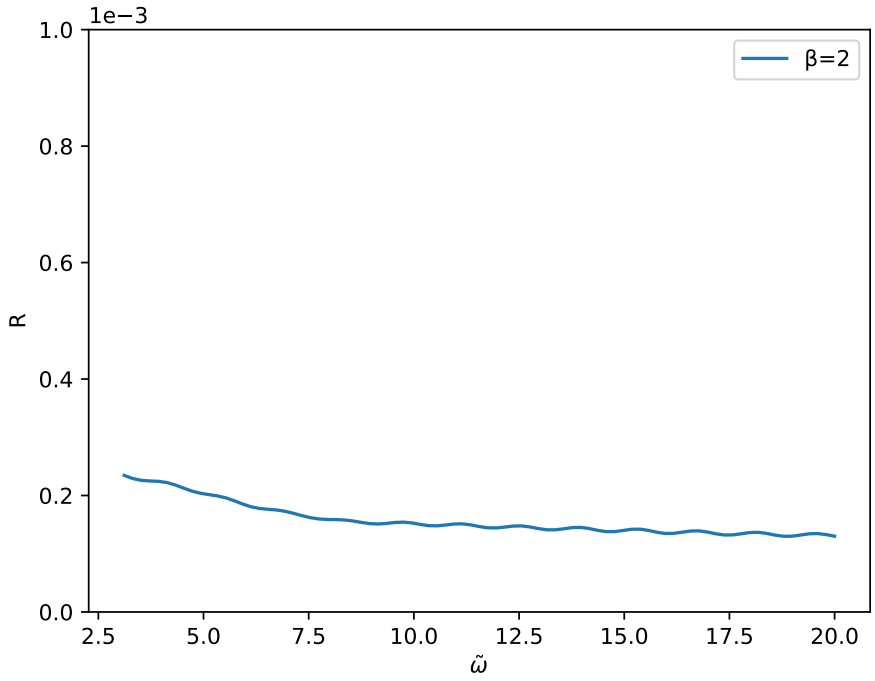

Figure 17. Reflectivity of strained graphene with $\beta = 2$.

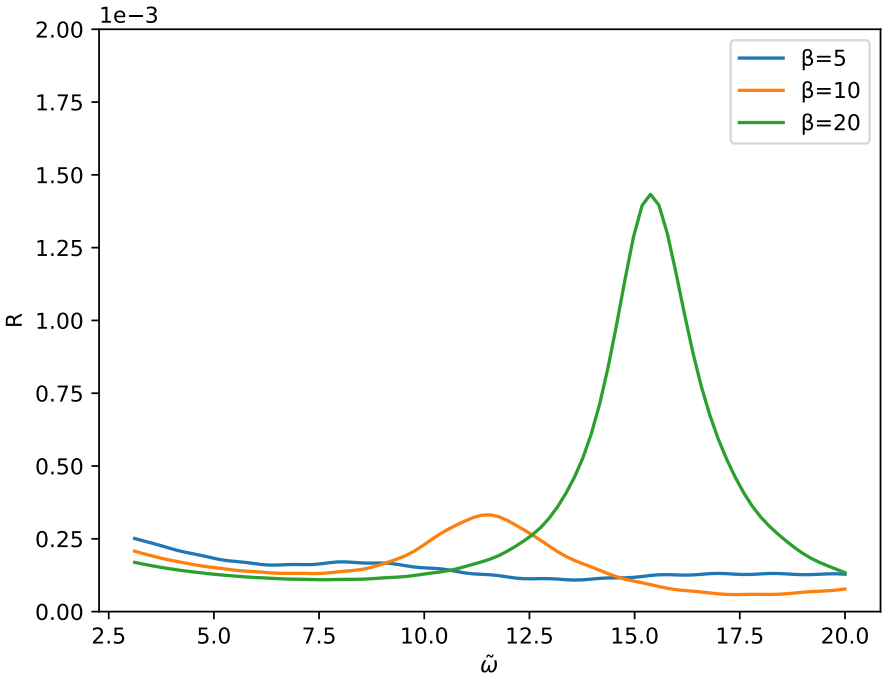

Figure 18. Reflectivity of strained graphene at $\theta = 0$.

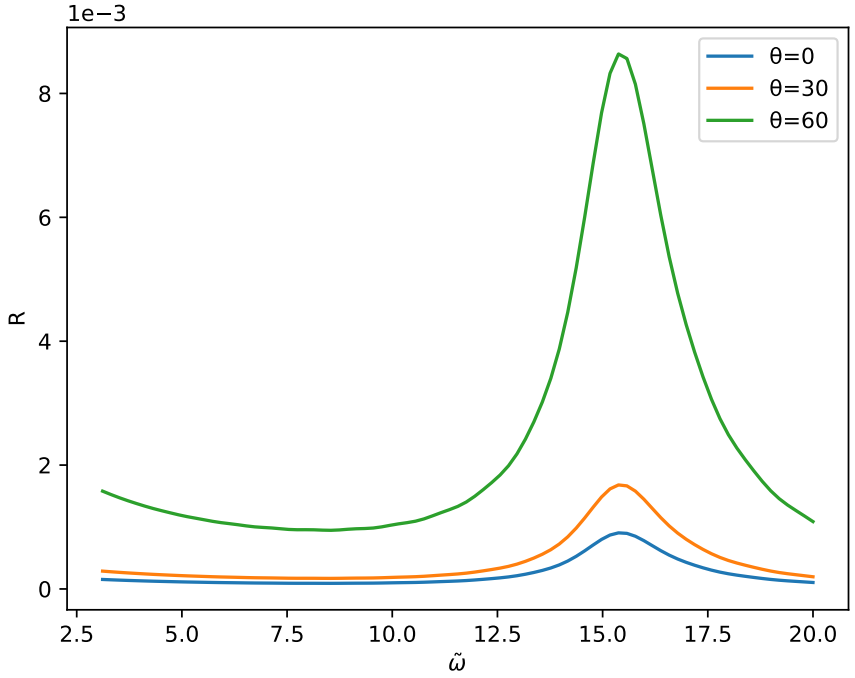

Figure 19. Reflectivity of s-polarised for graphene strained at $\beta = 20$.

Due to the imaginary component of conductivity, the calculated reflectivity for pristine graphene appears higher at $\tilde{\omega} < 7$ but then approaches the correct value. The same effect appears for strained graphene. Luckily, the interesting peaks due to strain arise at higher values of $\tilde{\omega}$, which suggests they are unaffected by these inaccuracies, and experiments can still look for such peaks at $\tilde{\omega} > 7$ for strained graphene.

The patterns for conductivity shown in figure 14 can be explained using the energy spectra in figures 5 and 6; as the bands become flatter with higher values of β, the energy differences between energy bands tend to become more uniform. In figures 20, and 21, the bands for various energy levels are shown, and as the density of states becomes higher near $q_y = 0$, the energy differences near this point becomes more significant and show up as a peak in the plot of conductivity. The figures show a pattern where the peaks become narrower, higher, and closer to the values of ΔE as the value of β becomes higher; this should be expected since the flattening of the bands becomes stronger as the amplitude of the strain increases.

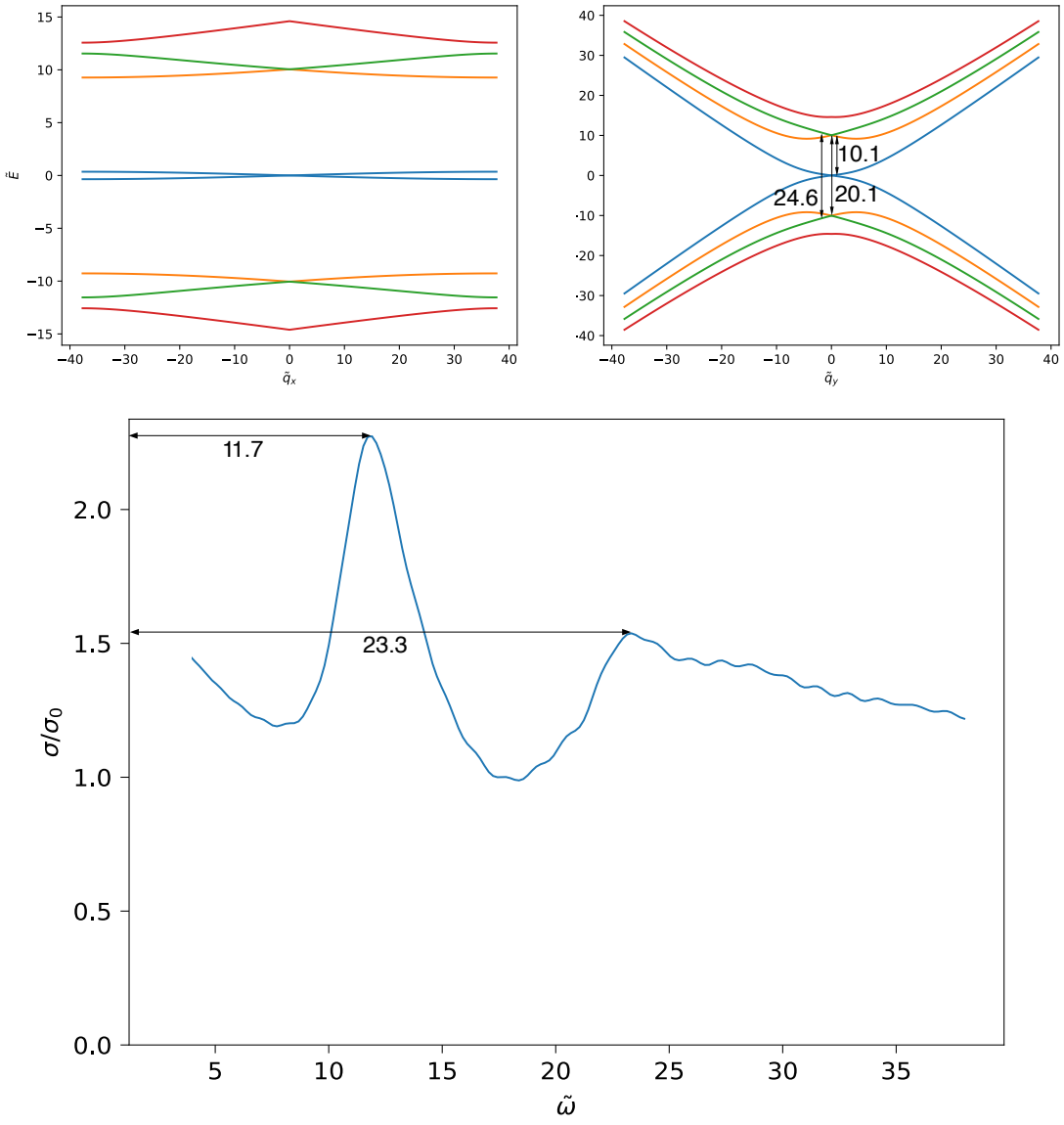

Figure 20. Energy levels at $\beta = 10$ as functions of q_x (top left) and q_y (top right). σ/σ_0 for a higher range of $\tilde{\omega}$ for $\beta = 10$ (bottom)

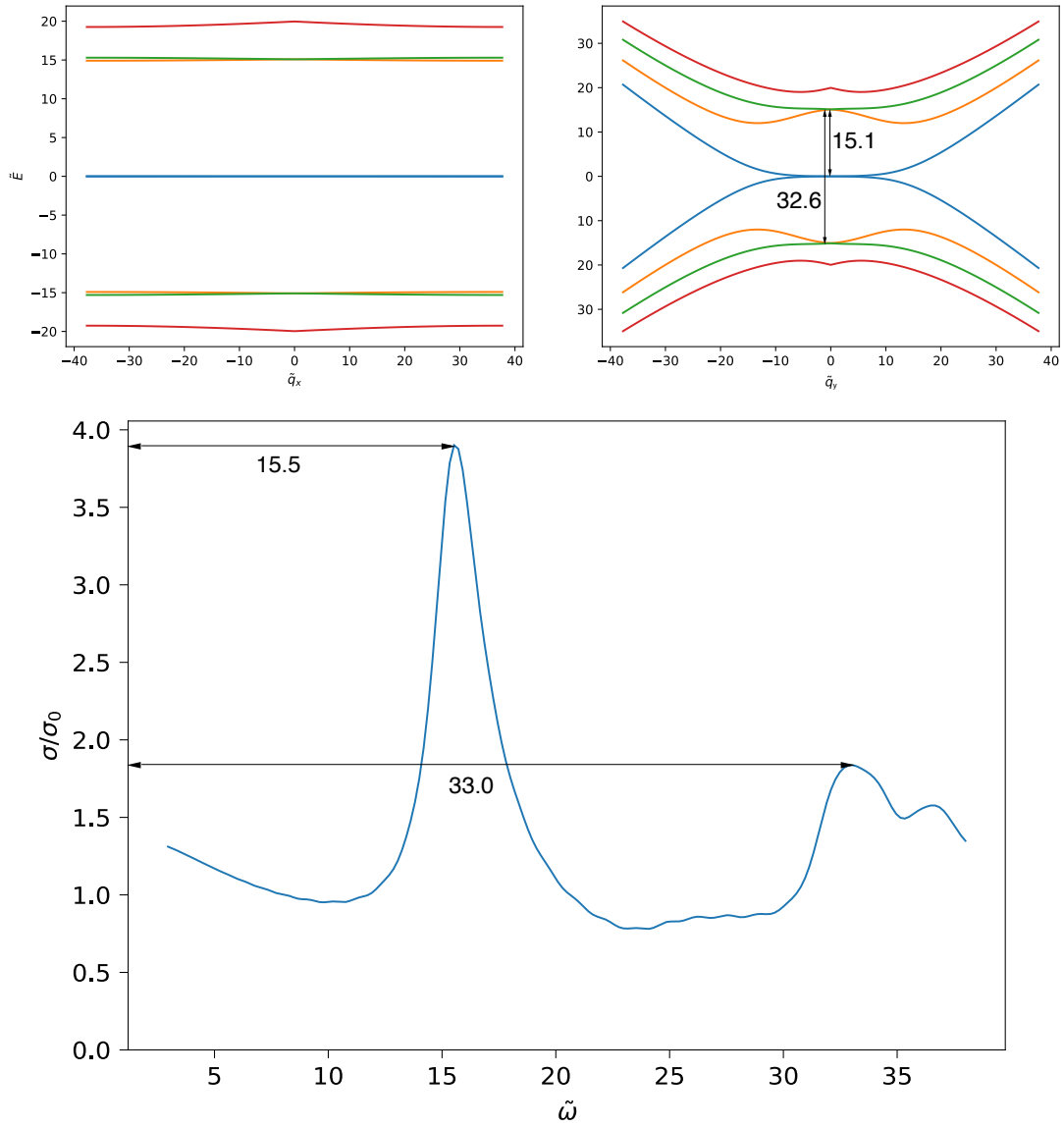

Figure 21. Energy levels at $\beta = 20$ as functions of q_x (top left) and q_y (top right). σ/σ_0 for a higher range of $\tilde{\omega}$ for $\beta = 20$ (bottom)

7 Conclusion

The reasonable agreement of the calculated conductivity for bare graphene with the known value of σ_0, as well as the continuous deviation from that value as the strain increases give good support to the obtained results. Numerical artifacts such as the value for conductivity of pristine graphene approaching σ_0 but not exactly equalling it, as well as the oscillation of the values at low values of β can all be varied with the selected parameters in the calculation.

The effect on the real component of conductivity at low values of $\tilde{\omega}$ for bare graphene can be expected at non-zero temperatures [13], and also has a contribution from the calculation method selected to avoid the divergence at low frequencies. A similar effect should be expected for strained graphene as explained above. Thus results for low frequencies that were influenced by the omission of low energy differences can be omitted.

The results for reflectivity follow directly from the conductivity, though they are related to the absolute value of the optical conductivity rather than the real component. The predicted values for reflectivity can be tested experimentally for different values of the period of strain L and angle of incidence θ. The artificial increase in reflectivity at low frequencies does not interfere with the peaks, which even for $\beta = 5$ appear at higher frequencies; this suggests that such artifacts should not significantly influence the predictions for the location, height, and width of the peaks, so it remains possible to test them experimentally. The effect of strain on reflectivity may be amplified by varying the angle of incidence in the case of s-polarised light; as shown above, a higher angle of incidence amplifies the conductivity peaks which could make them easier to detect experimentally.

Since the aim was to find whether it is possible to detect strain in graphene using its optical properties, the results indicate that, especially for higher amplitudes of strain, it is possible to detect the change in graphene's reflectivity due to strain. The period of the strain can be seen in the scaling of the frequency, while the maximum value for the conductivity/reflectivity is an indicator of the strain amplitude.

The calculations show a relationship between flat bands, which result from strain, and the optical conductivity and reflectivity. Measurements of reflectivity at dif-

ferent strain amplitudes may be used to verify and test the accuracy and possible limitations of these predictions.

As expected, the value of the conductivity shows higher peaks for flat bands at higher strain amplitudes. It is reasonable to expect higher and sharper peaks at higher values of strain due to the energy bands flattening; this can be experimentally verified by measuring the reflectivity for higher strain amplitudes.

Since I study in-plane strain here, an obvious way to expand upon the current results is to calculate the same results for out-of-plane strain, as well as the combined effect of in-plane and out-of-plane strain. In addition, different forms of periodic strain can be calculated other than the cos-shaped strain presented here.

References

[1] K. S. Novoselov et al. “Electric Field Effect in Atomically Thin Carbon Films”. In: *Science* 306.5696 (2004), pp. 666–669. DOI: 10.1126/science.1102896. eprint: https://www.science.org/doi/pdf/10.1126/science.1102896. URL: https://www.science.org/doi/abs/10.1126/science.1102896.

[2] C. Lee et al. “Measurement of the Elastic Properties and Intrinsic Strength of Monolayer Graphene”. In: *Science (New York, N.Y.)* 321 (July 2008), pp. 385–8. DOI: 10.1126/science.1157996.

[3] M. S. e. a. Novoselov K. Geim A. “Two-dimensional gas of massless Dirac fermions in graphene”. In: *Nature* 438 (Nov. 2005), pp. 197–299.

[4] R. Raveendran-Nair et al. “Fine Structure Constant Defines Visual Transparency of Graphene”. In: *Science (New York, N.Y.)* 320 (July 2008), p. 1308. DOI: 10.1126/science.1156965.

[5] C. Si, Z. Sun, and F. Liu. “Strain engineering of graphene: a review”. In: *Nanoscale* 8 (6 2016), pp. 3207–3217. DOI: 10.1039/C5NR07755A. URL: http://dx.doi.org/10.1039/C5NR07755A.

[6] M. Liu et al. “Fundamental Insights into Graphene Strain Sensing”. In: *Nano Letters* 21.1 (2021). PMID: 33372510, pp. 833–839. DOI: 10.1021/acs.nanolett.0c04577. eprint: https://doi.org/10.1021/acs.nanolett.0c04577. URL: https://doi.org/10.1021/acs.nanolett.0c04577.

[7] V. J. Kauppila, F. Aikebaier, and T. T. Heikkilä. “Flat-band superconductivity in strained Dirac materials”. In: *Phys. Rev. B* 93 (21 June 2016), p. 214505. DOI: 10.1103/PhysRevB.93.214505. URL: https://link.aps.org/doi/10.1103/PhysRevB.93.214505.

[8] C. Kittel. *Introduction to Solid State Physics*. 8th ed. Wiley, 2004. ISBN: 9780471415268.

[9] M. I. Katsnelson. *Graphene: Carbon in Two Dimensions*. Cambridge University Press, 2012. DOI: 10.1017/CBO9781139031080.

[10] F. de Juan, M. Sturla, and M. A. H. Vozmediano. “Space Dependent Fermi Velocity in Strained Graphene”. In: *Phys. Rev. Lett.* 108 (22 May 2012), p. 227205. DOI: 10.1103/PhysRevLett.108.227205. URL: https://link.aps.org/doi/10.1103/PhysRevLett.108.227205.

[11] R. Banerjee et al. “Strain Modulated Superlattices in Graphene”. In: *Nano Letters* 20.5 (2020). PMID: 32134680, pp. 3113–3121. DOI: 10.1021/acs.nanolett.9b05108. eprint: https://doi.org/10.1021/acs.nanolett.9b05108. URL: https://doi.org/10.1021/acs.nanolett.9b05108.

[12] P. Koskinen et al. “Optically Forged Diffraction-Unlimited Ripples in Graphene”. In: *The Journal of Physical Chemistry Letters* 9.21 (2018), pp. 6179–6184. DOI: 10.1021/acs.jpclett.8b02461. eprint: https://doi.org/10.1021/acs.jpclett.8b02461. URL: https://doi.org/10.1021/acs.jpclett.8b02461.

[13] T. Stauber, N. M. R. Peres, and A. K. Geim. “Optical conductivity of graphene in the visible region of the spectrum”. In: *Phys. Rev. B* 78 (8 Aug. 2008), p. 085432. DOI: 10.1103/PhysRevB.78.085432. URL: https://link.aps.org/doi/10.1103/PhysRevB.78.085432.